FEASIBILITY OF A JET-STIRRED REACTOR FOR EVALUATING REPLACEMENTS FOR HALON FIRE RETARDANTS

BY

JON CYBULSKI

A thesis submitted in partial fulfillment

of the requirement for the degree of

Master of Science in Mechanical Engineering

University of Washington

1994

Approved by _____
Chairperson of Supervisory Committee

Program Authorized
to Offer Degree Mechanical Engineering

Date December 14, 1994

Master's Thesis

In presenting this thesis in partial fulfillment of the requirements for a Master's degree at the University of Washington, I agree that the Library shall make its copies freely available for inspection. I further agree that extensive copying of this thesis is allowable only for scholarly purposes, consistent with "fair use" as prescribed in the U.S. Copyright Law. Any other reproduction for any purposes or by any means shall not be allowed without my written permission:

Signature Jon Applebaum

Date 12/14/94

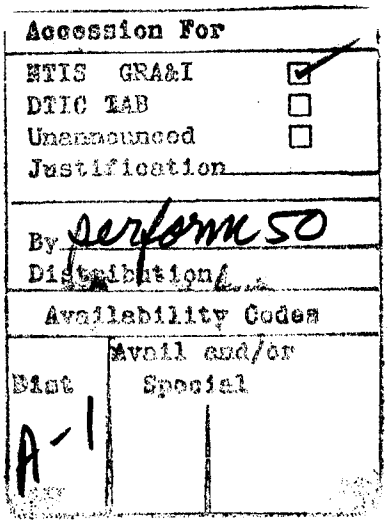

TABLE OF CONTENTS

LIST OF TABLES

Number *Page*

LIST OF FIGURES

Number *Page*

ACKNOWLEDGMENTS

The author wishes to express sincere appreciation to Professor Kramlich for his assistance in completing the research. Due to the relatively short timeframe available, Professor Kramlich provided valuable assistance in completing the computer modeling. This assistance significantly helped in completing the research and manuscript on time.

CHAPTER I: BACKGROUND AND EXPERIMENTAL OBJECTIVES

Background

Halons have been used as extinguishing agents for over 20 years. This type of fire suppression dates back to the late 1930's and 1940's when researchers discovered that halogenated methanes reduced flame velocities and inhibited ignition (Zentler-Gordon, 1940). Further research resulted in the development of commercial halogenated fire suppression agents.

The two most popular halons are Halon 1301 (CF_3Br) and Halon 1211 (CF_2BrCl). Halon 1301 is mainly used in fixed location discharge stations due to its low boiling point (-58 C). The higher boiling point of Halon 1211 (24 C) has made it popular with portable fire extinguisher applications. The principal advantages of halons are their low extinguishing concentration requirements and relatively non-toxic byproducts. One important benefit is that they do not damage equipment, which is critical in aircraft, computer facilities and nuclear plant electrical control rooms.

Halon 1301 and 1211 have been extremely successful fire extinguishing agents. Unfortunately for fire suppression, they are being phased out due to their adverse impact on the stratospheric ozone (Senecal, 1992). The stability of these retardants in the troposhpere results in their diffusion into the stratosphere where they break down to yield chlorine and bromine. The chlorine and bromine atoms then react with O_3 resulting in loss of stratospheric ozone. Under the latest

amendments to the Montreal Protocol on Substances That Deplete the Ozone Layer, the production of halons was banned as of 1 January 1994 except for limited applications where no viable alternative exists (Chemical & Engineering News, 1 March 1993). Therefore, research leading to the development of halon alternatives has become vitally important.

Mechanisms of Fire Suppression

To provide background on the behavior of halons, a brief discussion on flame destabilization is needed. Fire suppressants destabilize flames by at least two mechanisms:

a. Radiative heat feedback is necessary to evaporate or devolatilize sufficient fuel to support the flame. The use of a suppressant can reduce the amount of heat feedback by simply diluting and elongating the flame. The reduced feedback is due to the increased beam length for radiative transport and the reduced direct exchange area. Continued feedback reduction will result in flame extinction.

b. A reduction in the global chemical reaction rate will leave more flamelets at strain levels beyond their extinction limit. This delays the overall reaction leading to an increase in flame length. Beyond the critical limit, the flame will no longer propagate.

These physical and chemical processes are tightly coupled in practical fire suppression experiments just as they are in a practical flame. Various suppressants proportion their action differently between the two mechanisms. Halon 1301 and

1211 mainly extinguish flames by reducing the global chemical reaction rate.

Gaseous fire retardants have routinely been evaluated using the cup burner test. Here, air flows around the outside of a cup that contains liquid fuel, with the cup supporting a diffusion flame. Retardant is then added to the air stream with the concentration at the point of extinction noted as a measure of retardant effectiveness. This test provides realistic representations of the mechanisms described above and gives good empirical guidance on flame suppression performance. However, the cup burner test does not permit an understanding of the relative importance of physical and chemical mechanisms. Therefore, an alternative method is needed in order to better understand the chemistry.

Halogenated Flame Chemistry

The flame suppression chemistry of halon 1301 has as its basis the activity of the halogen, bromine. The influence of this additive on flame speed, flame structure, and ignition delay has been extensively studied (Safieh *et al.*, 1982). The work has resulted in the identification of most of the critical reactions associated with the following halogen radical scavenging cycle:

$$CF_3Br + H \rightarrow CF_3 + HBr$$

$$O + HBr \rightarrow Br + OH$$

$$OH + HBr \rightarrow Br + H_2O$$

$$H + HBr \rightarrow Br + H_2$$

$$Br + Br + M \rightarrow Br_2 + M$$

$$H + Br_2 \rightarrow HBr + Br$$

$$H + Br + M \rightarrow HBr + M$$

The bromine (Br) atom also can abstract hydrogen from the parent hydrocarbon fuel, methane in this case, and regenerate HBr for another cycle:

$$CH_4 + Br \rightarrow CH_3 + HBr$$

This radical scavenging cycle shuttles bromine between Br and HBr. The net loss in chain carriers provides the main basis for reduction in the global chemical reaction rate which results in combustion extinction.

The CF_3 radical generated above can also abstract hydrogen from the parent molecule:

$$CH_4 + CF_3 \rightarrow CH_3 + CF_3H$$

Kinetic modeling of the CF_3 radical generated by the above reactions indicate that it also has fire suppression characteristics. The role of this radical can be evaluated by studying the behavior of CF_3H additive:

$$CF_3H + H \rightarrow CF_3 + H_2$$

$$CF_3H + OH \rightarrow CF_3 + H_2O$$

$$CF_3 + OH \rightarrow CF_2O + HF$$

$$CF_2O + H \rightarrow CFO + HF$$

There is doubt, however, whether the carbonyl fluoride (CF_2O) reaction proceeds rapidly enough to influence suppression (Safieh *et al.*, 1982). Unlike HBr, the high electronegativity of fluorine does not allow sufficient reaction of HF via:

$$OH + HF \rightarrow F + H_2O$$

Therefore, CF_3H does not develop a radical scavenging cycle, and its flame suppression performance is reduced relative to halon 1301.

Chlorine inhibition of flames has also been extensively studied (e.g., Xieqi *et al.*, 1993, Koshland *et al.*, 1992, Brouwer *et al.*, 1992). In these studies, two effects were noted:

a. The presence of the chlorine acts to scavenge chain carriers as described previously for HBr. This tends to reduce the CO oxidation rate and the rate of heat release.

b. Chlorine atoms also act as agents for the abstraction of hydrogen from hydrocarbon molecules:

$$R\text{-}H + Cl \rightarrow R\text{-} + HCl$$

The attacks on the parent fuel molecules by HBr and HCl along with the suppression of the oxidation of CO (CO + OH), leads to enhanced hydrocarbon intermediates and higher CO concentrations, and it leads towards flame extinction (Brouwer *et al.*, 1992).

Experimental Objective

The main objective was to conduct preliminary experiments which would lead the way in the development of a chemical kinetic database on the flame behavior of fluorinated halon replacement compounds. This was accomplished through the analysis of the combustion of simple fuels with halon additives in a jet-stirred reactor. This analysis was compared

with computer modeling.

The chemical kinetic database for fluorinated compounds in general is much weaker than it is for hydrocarbons or chlorinated organic compounds. Consequently, there is a need for experiments that generate global kinetic data against which kinetic models can be developed and verified. The global kinetic data for these experiments was generated through the use of a well-stirred reactor model.

The experiments addressed the flame chemistry of simple retardant compounds (CF_3Br and CF_3H) operating against methane fuel (CH_4). Two retardants were used so that the kinetic modeling for CF_3H and CF_3Br reactions could be studied. The kinetic model used for CF_3Br included reactions for CF_3H since Halon 1301 generates both the CF_3 and HBr radicals during combustion reactions. Therefore, by analyzing data using the two separate retardants, the overall behavior of the kinetic model could be studied.

The principal objective was to determine whether the retardant flame chemistry could be adequately resolved using a jet-stirred reactor system and to compare data generated with kinetic modeling.

CHAPTER II: EXPERIMENTAL SETUP

Jet-Stirred Reactor (JSR) and Fuel/Air/Halon Delivery System

The jet-stirred reactor system used was similar to the one used by Corr *et al.* (1991) shown in Figure 1. The system consists of a jet-stirred reactor, sonic nozzle assembly, and pre-mixing chamber.

The JSR consists of a 15.8 cc volume atmospheric pressure reactor cavity as shown in Figure 1. The reactor cavity is circular and insulated, with eight ports located on the vertical walls. The top four ports provide access for sampling probes and thermocouples and the bottom four ports provide for gas exhaust.

The sonic nozzle assembly consists of a single center jet that creates an upward to outward mixing pattern. Upon recirculation, the hot, burning gases mix with fresh reactants which stabilizes the combustion. The nozzle is made of Inconel with a jet diameter of approximately 0.06 inches designed to accelerate the mixture to sonic velocities.

The pre-mixing chamber provides a means for mixing fuel, air and retardant prior to injection into the reactor through the nozzle block.

The single-jet reactor configuration is superior for physical probing because the most uniform region is near the reactor walls. Another advantage is the absence of wall effects. At a mean residence time of 4 ms, the stirred gases have only minimal time to contact the walls, even when considering the thin boundary layers induced by the high

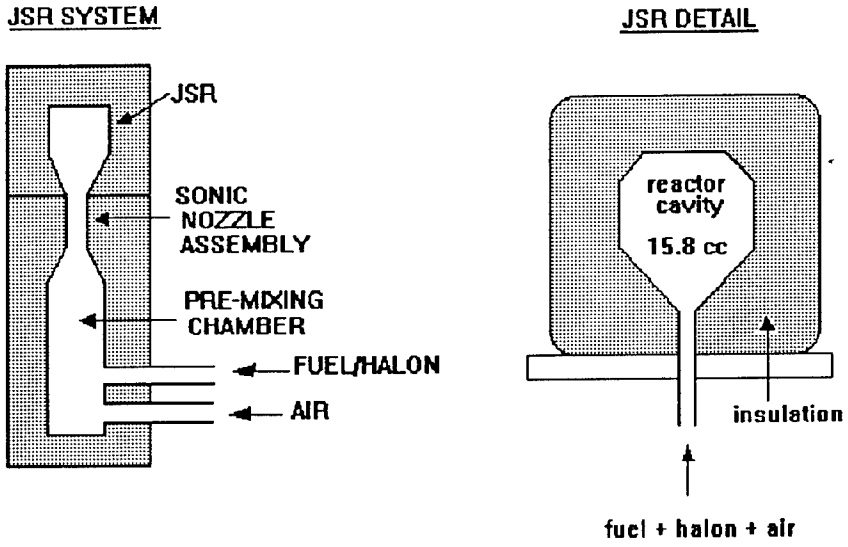

Figure 1: Jet-Stirred Reactor (JSR)

velocities used in the experiment. Although it is not possible to obtain perfectly stirred behavior, something that is never entirely achieved for high-temperature combustion, it is possible to obtain a reasonable degree of well-stirred behavior (i.e. experimentally uniform) which has been a critical component in the development of recent kinetic mechanisms for NOx chemistry (Miller and Bowman, 1989: Glarborg *et al.*, 1986). Consequently, use of a perfectly stirred model can be used as a reasonable first approximation

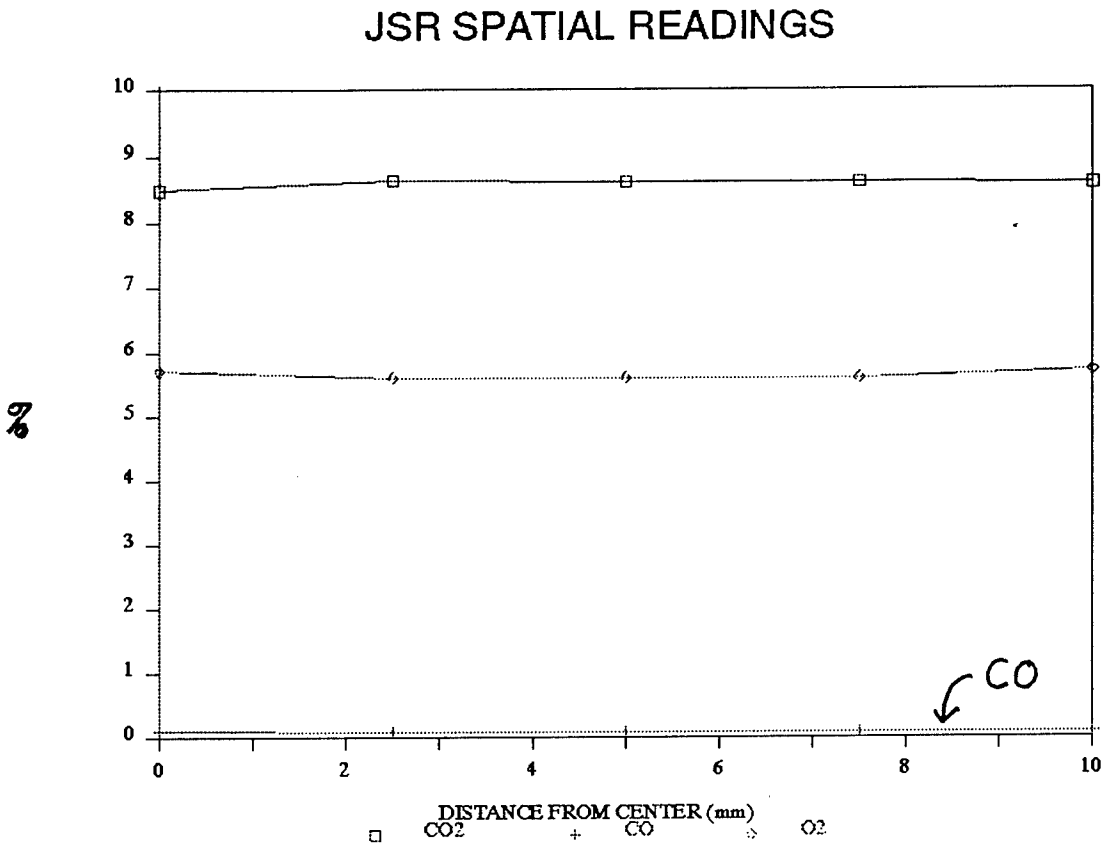

Figure 2: JSR Spatial Readings

for combustion analysis. In order to justify the assumption of well-stirred behavior in the JSR shown in Figure 1, spatial readings were taken at 0, 2.5, 5, 7.5 and 10 millimeters from the centerline (maximum diameter is 25 millimeters) of the JSR. The combustion mixture was CH_4/Air with 130% theoretical air using a mean residence time of 4 ms. Concentrations of CO_2, CO and O_2 were measured with no appreciable variations noted as shown in Figure 2.

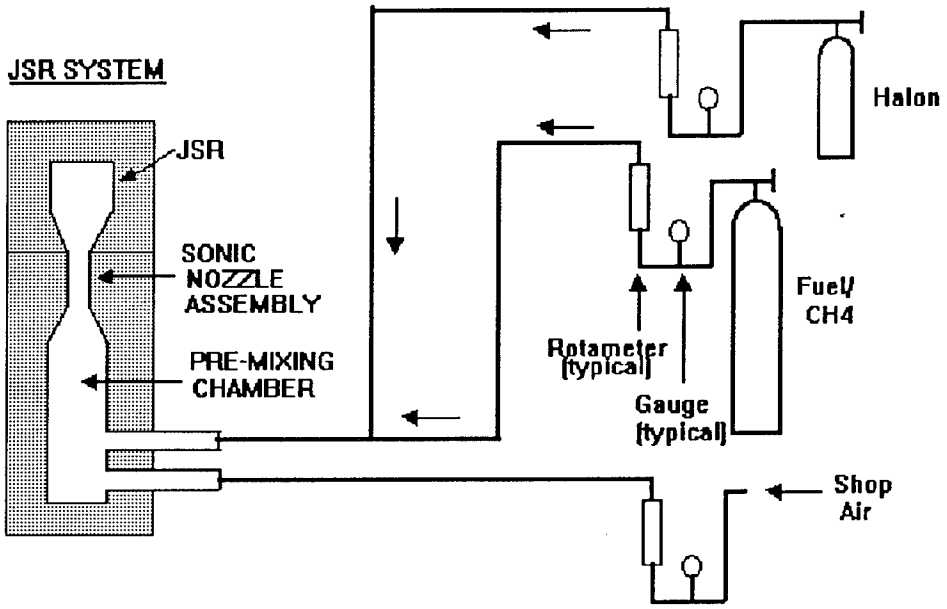

Figure 3: Fuel/Air/Halon Delivery System

All gas streams into the reactor system were controlled by the use of variable-area rotameters as shown in Figure 3. Descriptions of the flow rate handling system and its calibration data can be found in Appendix B.

A summary of reactor system operating conditions is as follows:

Parameter	Condition
Pre-mixing Chamber	20-25 psig
Mass Flow Rates	Based on % theoretical air as calculated in Appendices A & B
JSR Mean Residence Time	4 milliseconds (typical)

Sampling and Measurement System

Figure 4 provides a schematic of the sampling and measurement system. Gas samples were withdrawn using a water-cooled quartz micro-probe of the design used by Kramlich and Malte (1978). The tip of the probe was placed approximately 4-5 millimeters from the reactor centerline. The gas samples were maintained at approximately 0.27 atm in the probe to suppress further chemical reaction and were continuously pumped through a glass water trap cooled to 0 degrees C to ensure removal of water by condensation. The samples were then passed through a stainless steel bellows pump. See Chapter III for changes made to the sampling system due to difficulties encountered during the experiment.

A fitting used for sampling was located downstream of the pump outlet. Samples were withdrawn through this fitting with a gas tight syringe. The samples were then injected via a stainless steel line into the 1 cm^3 sample loop of the gas chromatograph (GC) described in Appendix C. A flame ionization detector (FID) was used to detect the presence of residual halons. The halons were identified by comparing GC retention times with those retention times determined by calibration. See Appendix C for details pertaining to GC-FID calibration methods and operating procedures.

After the sample fitting, the sample flow divided into a manifold and was routed through CO (Horiba), CO_2 (Horiba), O_2 (Servomex), and NO/NOX (TECO) gas analyzers. The gas analyzers

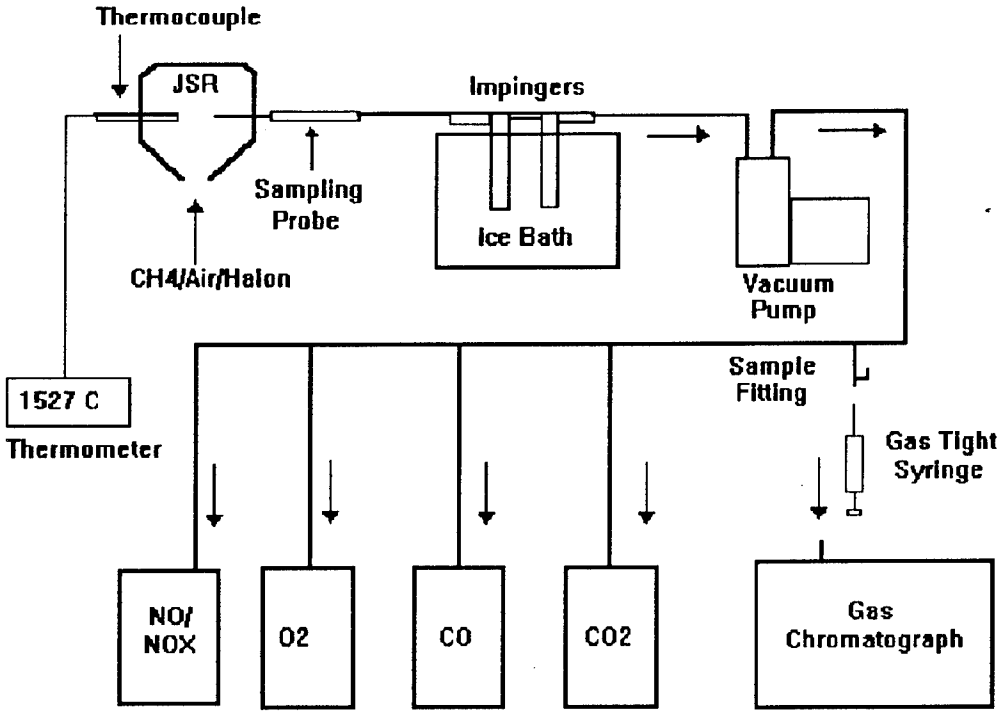

Figure 4: Sampling and Measurement System

were calibrated using span gas and nitrogen before each reactor run.

All interconnecting tubing used in the system was made of Teflon.

Temperature measurements in the JSR were taken using type R platinum-rhodium thermocouples and a Fluke electronic thermometer. The thermocouple tips were coated with a thin layer of material (BeO) which prevented catalytic reactions. The temperature readings were corrected to account for radiation losses.

Experimental Procedure

As discussed in Chapter I, the experimental objective was to analyze the flame bahavior of the fire retardant compounds, CF_3Br and CF_3H, operating against methane/air combustion. This was accomplished by varying the amount of halon gases injected and comparing the JSR concentrations of various compounds with concentrations calculated by computer kinetic modeling. Two general sets of experimental data were taken as described in the following paragraphs.

The first data set involved operating the JSR at a constant combustion temperature of approximately 1800 K. Halon gases were injected into the pre-mixing chamber. The combustion temperature was maintained by varying the methane flow rate which caused a variation in the theoretical air from approximately 120% to 135%. This data set was taken largely to screen the experimental procedure. Temperature, O_2, CO, and CO_2 readings were taken with halon gases injections at mole concentrations varying from 0 to 1.5%. Due to time and scheduling constraints, additional data at constant temperature with halon injections varying from 0 to 3% as well as NO/NOx and GC readings were not taken.

The second data set involved operating the JSR with methane/air flows maintained at 120% theoretical air and 4 ms residence time (See Appendix A for gas flow rate calculation). Halon gases were injected into the pre-mixing chamber at mole concentrations that varied from 0 to 3%. Data at 2.5% and 3.0%

halon 1301 concentrations were not taken due to flame extinguishment happening at 2.5%. At 120% theoretical air the combustion temperature dropped from 1820 to 1750 degrees Kelvin as halon 1301 the retardant flow was increased. For CF_3H, the combustion temperature increased from 1820 to 1850 as the retardant flow was increased. These high temperatures were necessary in order to prevent combustion failure due to the fire suppression characteristics of the halon gases. In addition to CO, O_2, CO_2 and temperature readings, NO/NOx and GC readings were taken.

The above data were analyzed as discussed in Chapter III. See Table 1 for a summary of the experimental matrix.

Kinetic Modeling

As discussed above, the two fire retardant compounds were operated against methane fuel. Methane fuel was used due to its well established kinetic model mechanism. The kinetic modeling was accomplished using the MARK-II Combustor Model developed by Professor D.T. Pratt at the University of Washington (1990). The Miller/Bowman mechanism (Miller and Bowman, 1989) was used with the exception of the N_2O+OH reaction rate which was reduced to reflect recent data from the Technical University of Denmark. The CF_3H reaction rates were taken from a recent compilation (Westmoreland *et al.*, 1994). For the CF_3Br kinetic modeling, the CF_3H reaction rates were augmented with the CF_3Br reactions from another recent compilation (Battin-Leclerc *et al.*, 1994). For the other CF_3Br

modeling set, the reaction rate for Br+Br+M from a 1982 compilation (Westbrook, 1982) was changed in the CF_3Br kinetic model from Battin-Leclerc *et al.*, 1994. NOx chemistry in all models included the extended Zeldovich mechanism, the N_2O mechanism, and a simplified prompt mechanism.

Table 1. Summary of Experimental Matrix:

OBJECTIVE	HALON	REMARKS
Operate Methane/Air at constant temperature	CF_3H	- Hold methane/air combustion temperature constant at ~1800 K by varying methane flow rate -4 ms mean residence time - Inject CF_3H at flow rates from 0% to 1.5% - Take readings at each CF_3H flow rate setting
Operate Methane/Air at constant temperature	CF_3Br	- Hold methane/air combustion temperature constant at ~1800 K by varying methane flow rate - 4 ms mean residence time - Inject CF_3Br at flow rates from 0% to 1.5% - Take readings at each CF_3Br flow rate setting
Operate Methane/Air at constant flow rate and compare with kinetic modeling	CF_3H	- Hold methane/air combustion flow rates constant at 120% theoretical air - 4 ms mean residence time - Vary CF_3H flow rate from 0% to 3% - Take readings & sample at each CF_3H flow rate setting
Operate Methane/Air at constant flow rate and compare with kinetic modeling	CF_3Br	- Hold methane/air combustion flow rates constant at 120% theoretical air - 4 ms mean residence time - Vary CF_3Br flow rate from 0% to 3% - Take readings & sample at each CF_3Br flow rate setting

CHAPTER III: RESULTS AND DISCUSSION

Constant Temperature Data

The constant temperature data listed in Appendix D were taken mainly as a preliminary test of the experimental system and procedure. As a result, this experimental run did not fully explore the desired range of percent halon injection (0 to 3%), and NO/NO_x data were not obtained. Even though the data were considered unreliable due to a leak in the pre-mixing chamber as explained below, these data did point out some problems with the experimental system.

The first problem involved the water-cooled glass quartz sampling probe. The probe tip was designed with an orifice (0.51 mm) that would reduce the sample pressure to 0.27 atm. The reduced pressure was designed to suppress further chemical reactions in the sample upon entering the probe. However, due to the high combustion temperatures experienced (> 1500 C) being approximately equal to the melting point of the glass probe, the orifice tip fused shut preventing further withdrawal of samples. The probe tip was then modified to remove the orifice. This resulted in a larger tip diameter (2 mm) with the sample pressure being reduced to only 10 psia. This higher pressure failed to adequately suppress chemical reactions which resulted in further oxidation of CO in the probe. Further, the probe deteriorated much faster than normal due presumably to attack of the halogens on the quartz. The result was severe pitting of the probe hot section.

The second problem involved ensuring reliable temperature data. The high temperature tended to degrade the thermocouple tip coating at a faster rate than normal. Consequently, increased catalytic reactions at the thermocouple tip caused false temperature readings. The solution was to change thermocouples frequently during experimentation and monitor the coating breakdown. Three thermocouples were made for the "Constant Flow Rate" runs in order to ensure more reliable temperature data. The coating diameters on the thermocouple tips ranged from 1 to 1.8 mm. During the "Constant Flow Rate" runs, the two thermocouples with tip diameters less than 1.8 mm suffered coating breakdown immediately and could not be used for further data runs. Therefore, the remaining runs were accomplished with the 1.8 mm thermocouple which seemed to resist the high temperatures well.

The third problem encountered involved a substance that appeared in the sample tubing immediately after the impingers. Some of the substance also appeared after the vacuum pump. This caused concern because of the potential problems that could occur if this substance entered the gas analyzers. This substance was reddish dark-brown in color and was suspected to be residual Br_2 from the Halon 1301 experimental runs. The substance did not appear during the CF_3H experimental runs. The solution was to add two sets of impingers to the sample train. The additional impingers were

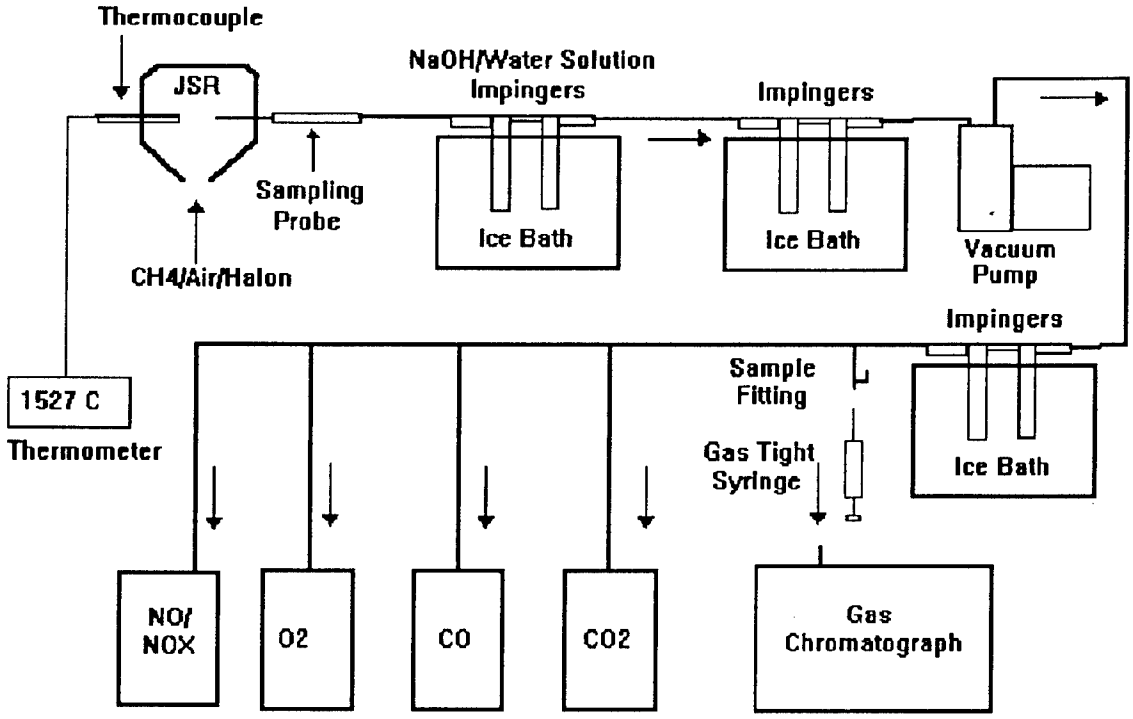

Figure 5: Modified Experimental System

placed before and after the vacuum pump as shown in Figure 5. Also in order to ensure that the acid gases were scrubbed from the gas sample, an $NaOH/H_2O$ solution was used in the first impinger set. This modified experimental system appeared to satisfactorily scrub out the brown substance and acid gases. However, the $NaOH/H_2O$ solution also removed part of the CO_2 which could potentially have an effect on the data readings. However, comparison of the base data for the "Constant Flow Rate" readings with the kinetic modeling did indicate that this loss was minor (approximately 0.1%).

Prior to addition of NaOH filled impingers, the acidic sample gas deteriorated the polished brass sample cell of one of the analyzers. This lead to signal degradation. Upon discovery, the problem was remedied by replacing the brass sample cell.

The final problem was a leak encountered in the pre-mixing chamber as discussed in Appendix D. This problem was quickly corrected but resulted in a reduction in the accuracy of the initial constant temperature run data. Due to time and scheduling constraints, additional data for constant temperature conditions were not obtained.

Constant Flow Rate Data

The constant flow rate data are listed in Appendix D. Data measurements were taken for CO, CO_2, O_2, and NO/NOx concentrations along with GC-FID sample analysis. CO concentrations were used as a direct indicator of retardant action. CO_2 and O_2 concentrations were used to verify stoichiometry and data quality. NO/NOx data were used as an indirect measure of the influence of the retardants on the radical population as well as providing additional data for kinetic model comparison. GC-FID sample analysis was performed to measure residual halon concentrations, hydrocarbon intermediates and fluorinated intermediates. These data were compared with kinetic modeling as follows:

Halon 1301 Data

As discussed in Chapter I, Halon 1301 suppresses fires

due to reduction in the global chemical reaction rate mainly caused by radical scavenging characteristics of HBr. As discussed below, the following third body reaction provides the main link for the cycling of Br to HBr:

$$Br + Br + M \rightarrow Br_2 + M$$

Review of the kinetics showed that the recent model for CF_3Br reactions (Battin-Leclerc *et al.*, 1994) differed from the earlier model (Westbrook, 1982) mainly in the above reaction. As a result, changing the reaction rate constants in the kinetic model for this reaction resulted in substantially different results. To illustrate this, the following two separate reaction rates were used in the kinetic model:

$k = 1.0 \times 10^{16}$ (Westbrook, 1982)

$k = 7.48 \times 10^{13} \exp(1690/RT)$ (Battin-Leclerc *et al.*, 1994)

The Battin-Leclerc 1994 rate had little affect on CO oxidation while the faster Westbrook 1982 rate resulted in substantial reduction in CO oxidation as Halon 1301 was increased. In order to see the effect of temperature alone on CO oxidation, kinetic modeling at the experimental temperatures was accomplished without halon injection. As shown in Figure 6, the temperature variations only caused minor changes in CO oxidation. Figure 6 also compares the kinetic modeling with the experimental data.

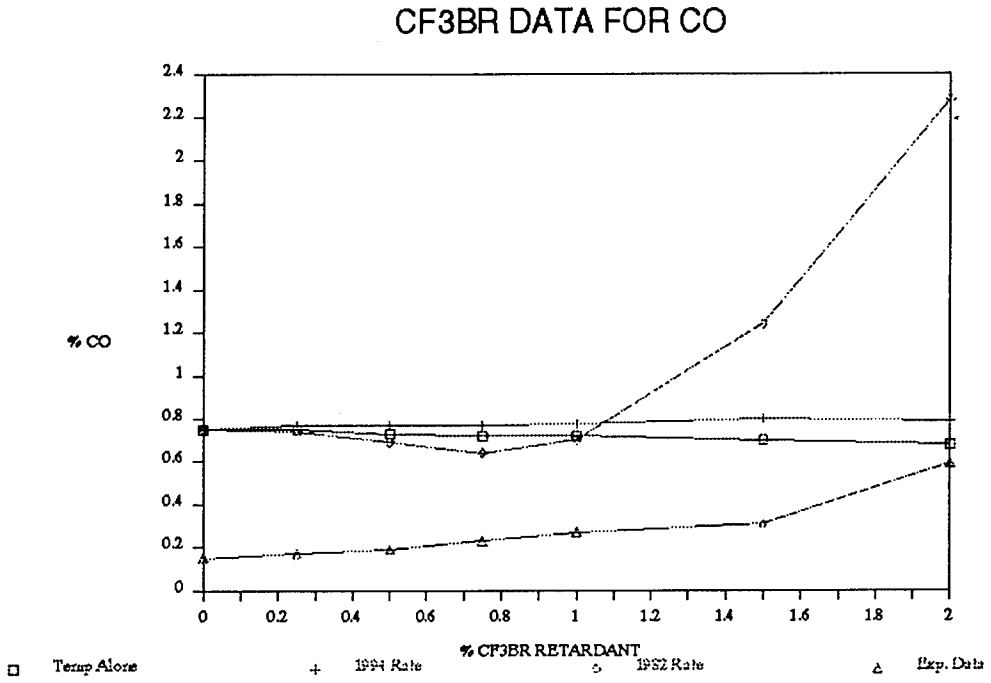

Figure 6: %CO as Halon 1301 concentration increases.

As discussed previously, the CO oxidation in the sample probe was apparent when comparing the experimental and kinetic data in Figure 6. Analysis of the potential CO oxidation in the probe using a simple plug-flow calculation with the base conditions (no halon) indicated approximately 0.30% absolute loss of CO. This suggested that the difference between the experimental and kinetic data could be attributed to CO oxidation in the probe. Nonetheless, the increase in CO for the experimental data shown in Figure 6 indicated that the reactor CO was also increasing. As a

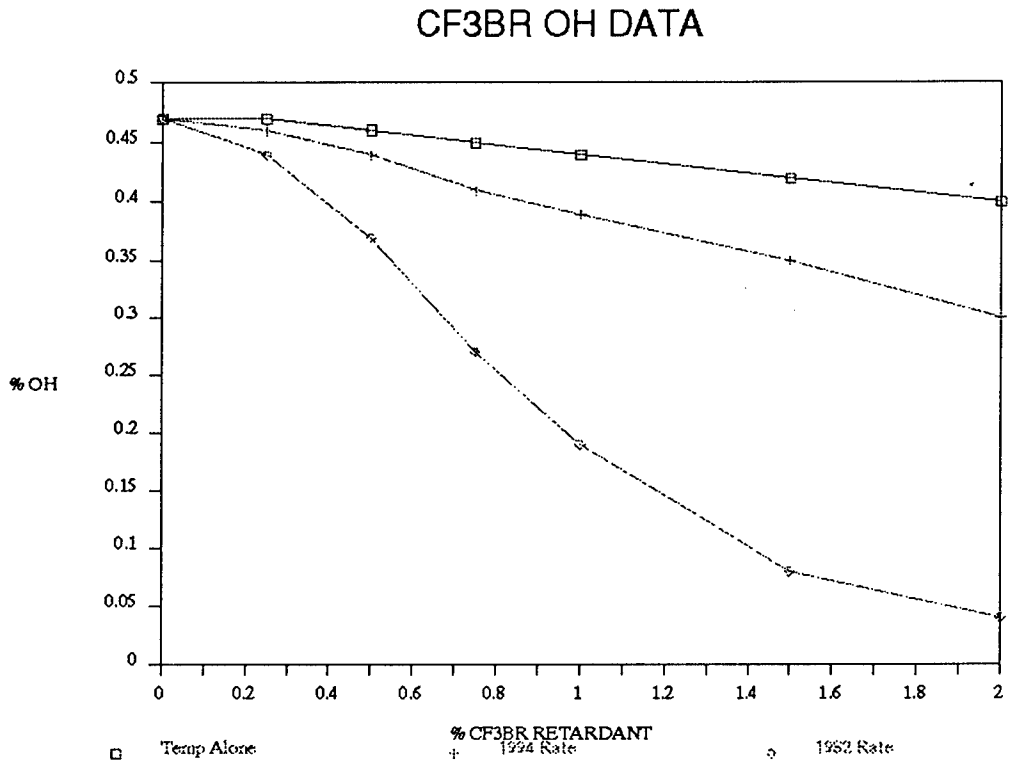

Figure 7: %OH as Halon 1301 concentration increases.

result, the relative CO increase as retardants were added was taken as being representative of the influence of the retardants on flame chemistry.

Based on comparison of the relative increases in CO, it was apparent that the kinetic models were not adequate. The 1994 rate resulted in little change as halon 1301 was increased. The 1982 rate resulted in little change initially with CO rapidly increasing after 1% halon 1301. This suggested that the reaction rate for Br+Br+M was not adequate or other parts of the model were inadequate. To

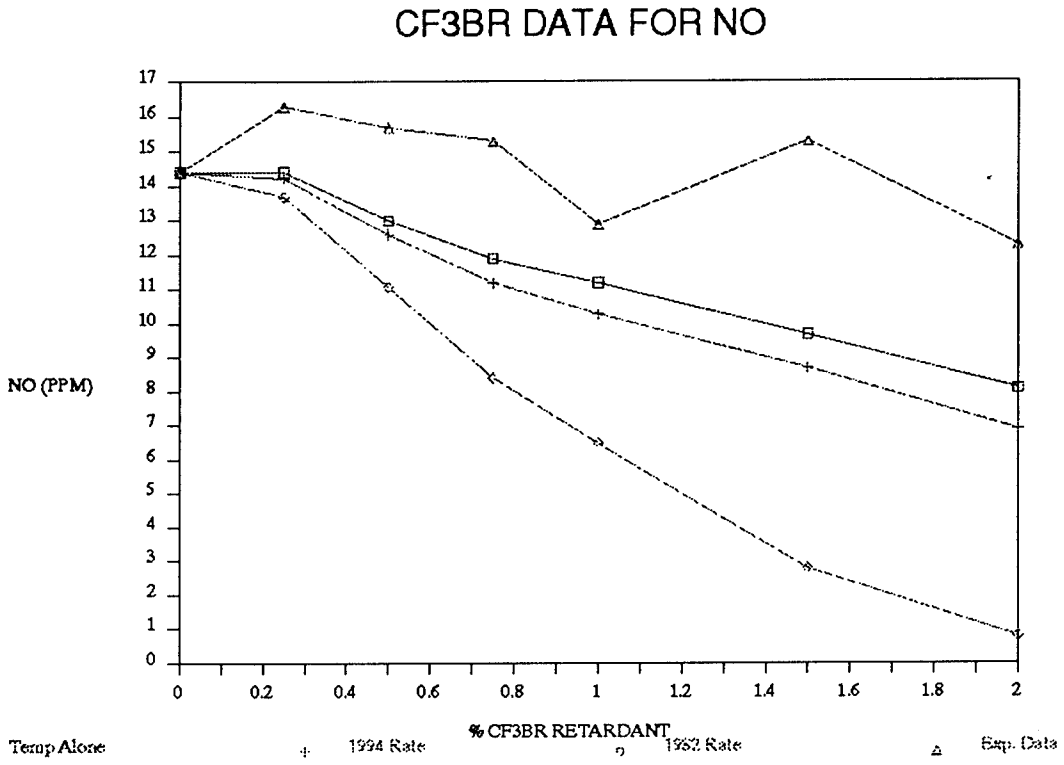

Figure 8: %NO as Halon 1301 concentration increases.

further illustrate this point, Figures 7 and 8 provide the comparison of data for OH and NO concentrations. Note that no experimental data for OH concentrations were obtained.

Figure 7 illustrates the reduction in OH mainly due to the HBr radical. This reduction in OH caused an increase in CO (see Figure 6) due to the reduced reaction of CO+OH. The 1982 rate caused a greater reduction while the 1994 rate caused a minor affect as halon was increased. As shown, the two rates differ substantially.

Figure 8 illustrates the affect of Br on NO formation.

Here the kinetic modeling does not seem to coincide with the experimental data where halon 1301 was increased from 0% to 0.25%. As shown by the experimental data, there was a slight increase initially with NO decreasing as halon 1301 was further increased. The kinetic model does not support this initial increase, however, it does suggest an initial "flatness". Additionally, experimental NO concentrations were also higher overall in comparison with the kinetic model concentrations. The fact that NO_x concentrations were higher than any of the computer model runs suggests the factors that were not well represented by the model were increasing NO_x. The data are somewhat complicated because of the sampling technique used. The data in Figure 8 were obtained using the NaOH scrubber for acid gas removal. This appears to have removed all NO_2 from the sample stream, since NO and NO_x readings from the analyzer were essentially identical. In preliminary runs, taken before the NaOH scrubber was introduced, NO_2 was observed to increase with halon addition, the total NO_x was seen to initially increase, and then decrease.

These observations suggest that halon promotes the formation of NO_x in a way that is not replicated by the model. One possible means would be an enhancement of CH concentrations, leading to additional prompt NO formation via $CH+N_2 \rightarrow HCN+N$, with the HCN and N eventually oxidizing to NO. One of the observed consequences of retardants is an

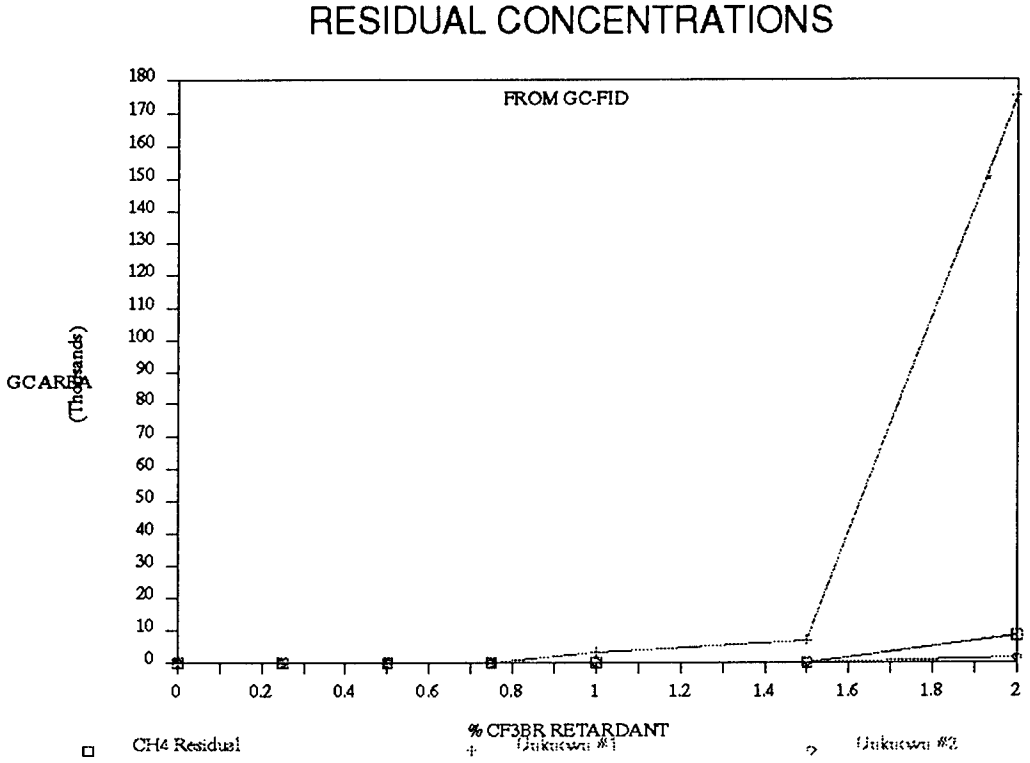

Figure 9: Residual concentrations from GC-FID

increase in hydrocarbon intermediate concentrations, potentially including CH.

GC-FID readings taken indicated no residual concentrations of halon 1301. However, measurable concentrations of other compounds appeared above 1% halon 1301. Figure 9 illustrates these concentrations based on GC peak area. As shown, one of the compounds was methane which increased as halon 1301 concentrations increased. Figure 10 illustrates methane concentrations from the kinetic modeling. As shown, the 1994 rate resulted in methane

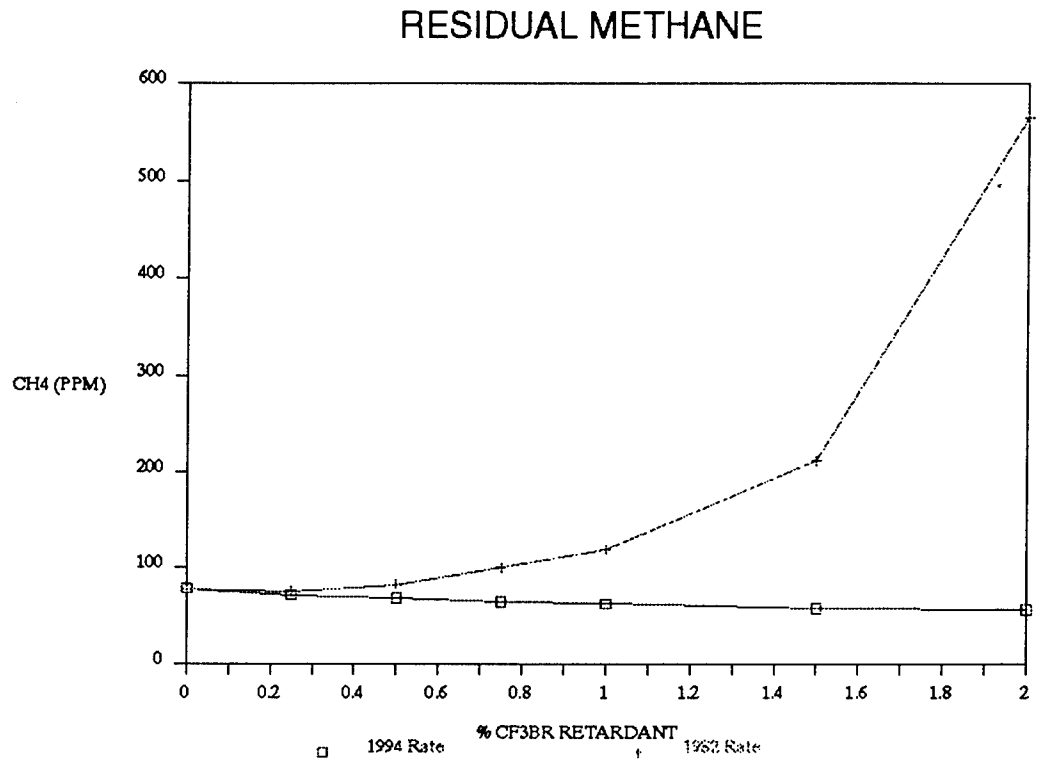

Figure 10: Residual methane from kinetic modeling.

decreasing while the 1982 rate resulted in methane increasing. Comparison of Figures 9 and 10 again illustrates that the kinetic modeling does not adequately predict the overall behavior. Note that the 1982 kinetics replicates part of the behavior in that methane does not start to significantly increase until 1.5% halon is added. Due to time constraints, further analysis of the other two unknown compounds in Figure 9 was not accomplished.

Consequently, the kinetic model for Br reactions appears to be weak as illustrated in Figures 6 through 10.

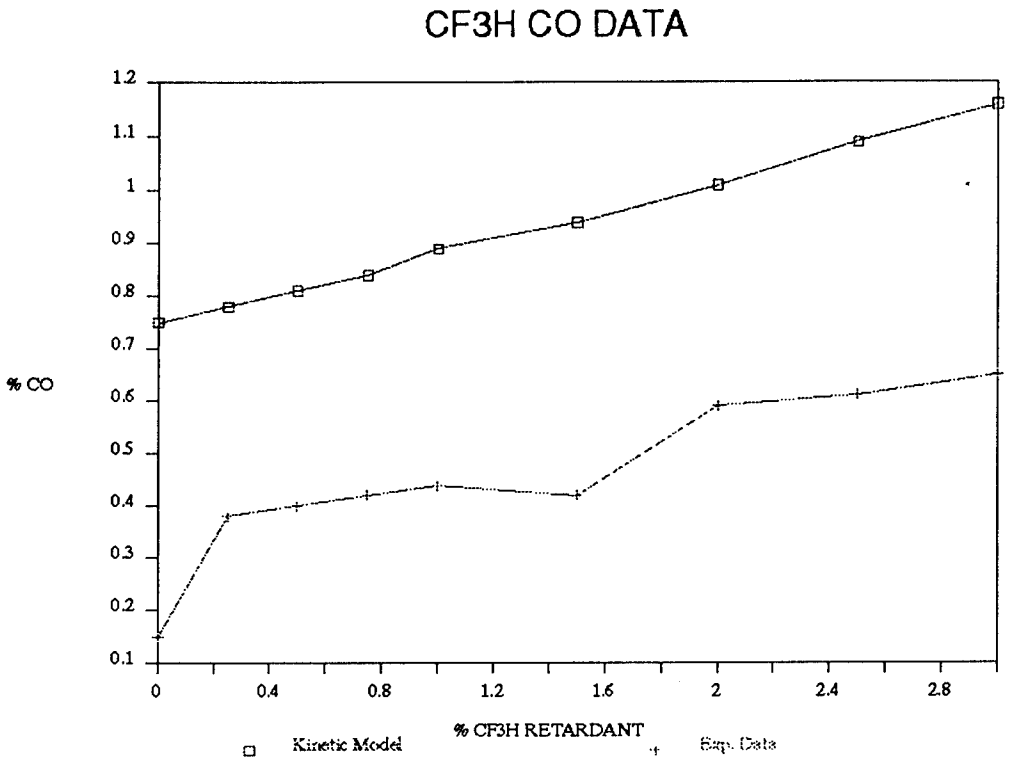

Figure 11: %CO as CF_3H concentration increases.

Modifying the Br+Br+M reaction rate may provide desirable results for reduced CO oxidation. However, the affect on NO generation requires further investigation.

Triflouromethane (CF_3H) Data

As discussed in Chapter I, the CF_3 radical appeared to have radical scavenging capabilities. The effects on CO oxidation were similar to the HBr radical. However, CF_3H lacked the radical scavenging cycle capabilities of the bromine in halon 1301.

Comparison of kinetic modeling with experimental data

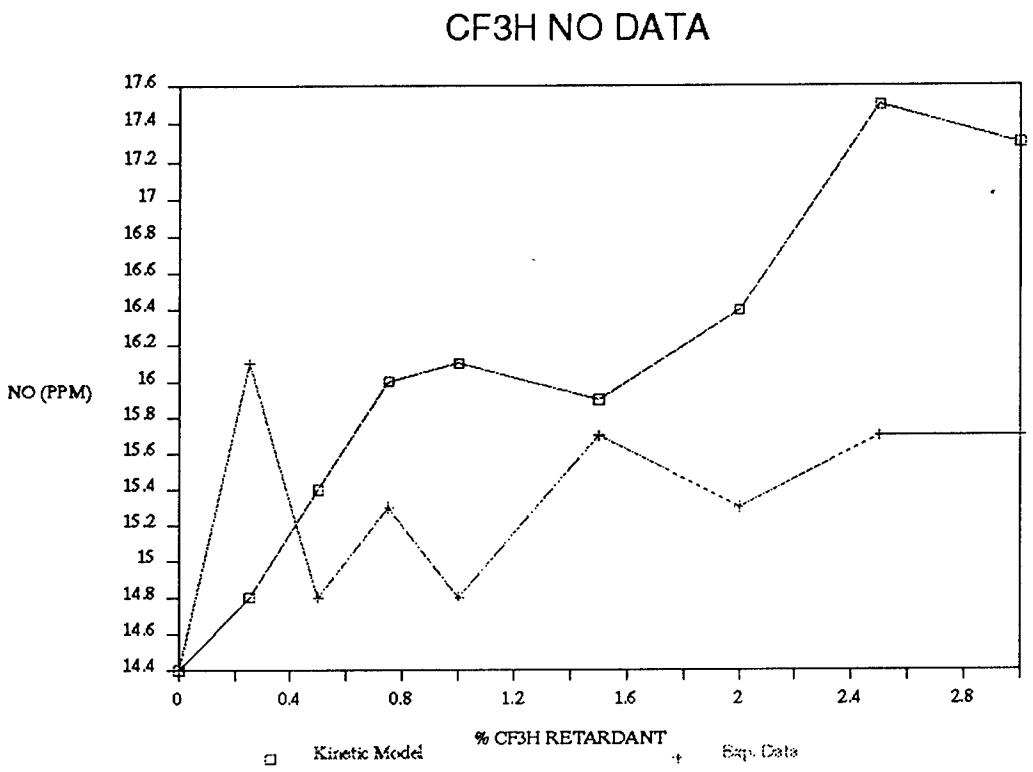

Figure 12: %NO as CF_3H concentration increases.

for CO oxidation showed the correct trend with respect to retardant loading. As shown in Figure 11, the relative increase in CO in the experimental data as CF_3H increased was similar to the kinetic model. However as discussed previously, due to CO oxidation in the sampling probe, the experimental data did not coincide with the kinetic model. Nevertheless, the relative increase appeared to be similar to the kinetic model.

Figures 12, 13 and 14 illustrate the changes in NO, O_2 and CO_2 as CF_3H was increased. Comparison of the

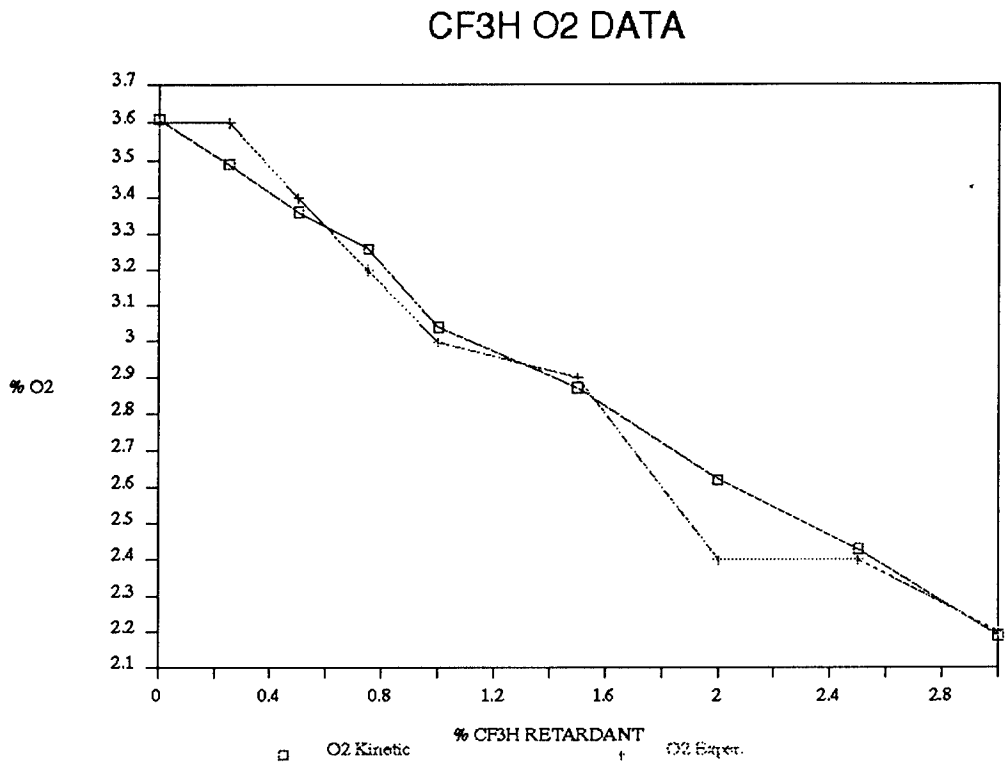

Figure 13: $\%O_2$ as CF_3H concentration increases.

experimental data with the kinetic model indicated that the model was in substantial agreement with the CO and O_2 experimental data. However, minor differences as triflouromethane was increased did exist for the NO and CO_2 data. Consequently, even though there appeared to be good agreement, the reaction rates for the CF_3H reactions provided by Westmoreland, *et. al.* (1994) require further research in order to verify their validity.

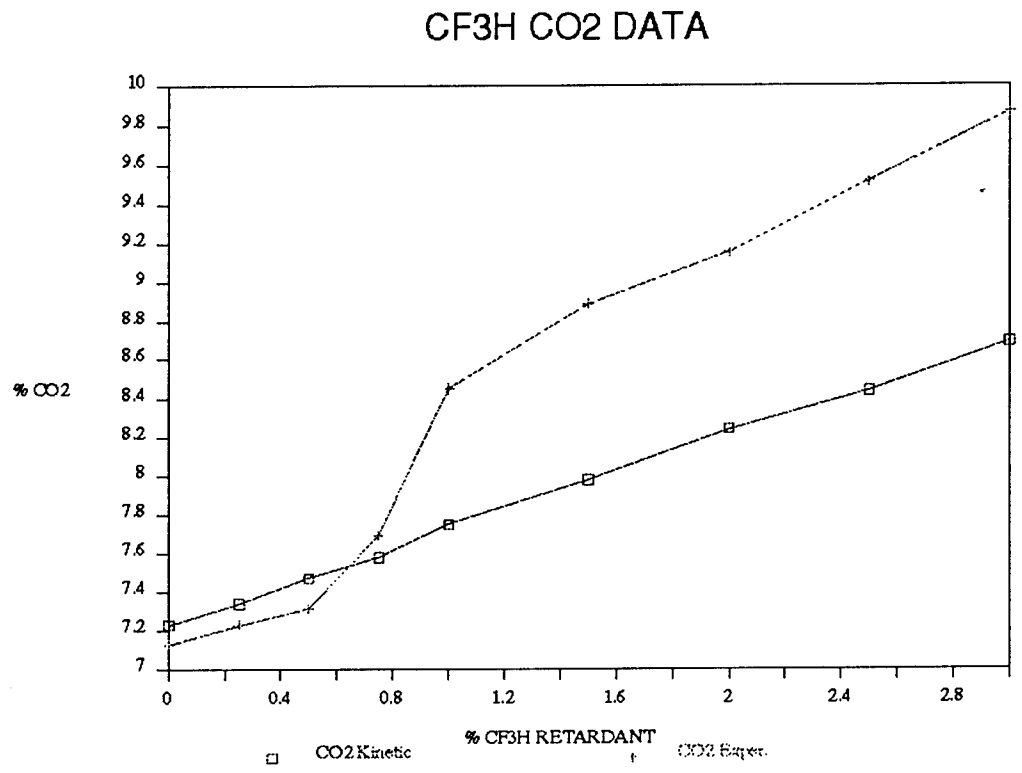

Figure 14: $\%CO_2$ as CF_3H concentration increases.

Conclusions

Based on the preceding discussions, using a JSR for analysis of halon gases should eventually be a reasonable method for study. The difficulties encountered as outlined in the preliminary test runs can be solved in order to provide satisfactory results. Proper analysis of CO oxidation in the probe will be important in order to properly correlate kinetic modeling with experimental results. An alternative would be to redesign the probe to minimize CO oxidation. A sufficient number of thermocouples

with adequately coated tips will also be necessary in order to ensure accurate temperature readings. However, the effect of Br_2 in the sample lines may require further study in order to satisfactorily solve this problem. The additional impingers and $NaOH/H_2O$ solution in the sample train appeared to solve the problem. However, the scrubbing can remove CO_2 and NO_2 causing further problems in analyzing the effect of halon retardants. Also, any bromine not removed by scrubbing could damage the analyzer equipment.

The CF_3H reaction rates provided by Westmoreland *et. al.* (1994) appeared to be in good agreement with the experimental data. Although, further research is required in order to ensure their validity.

The Br+Br+M reaction rates provided by Westbrook (1982) and Battin-Leclerc *et al.* (1994), however, did not correlate well with the experimental data. This was evidenced by the substantial differences in the increases in CO as shown in Figure 5. Therefore, further research in this area will be required in order to develop a kinetic model that adequately represents the Br reactions.

LITERATURE CITED

1. Battin-Leclerc, F., G.M. Come and F. Baronnet, "The inhibiting effect of CF_3Br on the Reaction of CH_4-O_2 at 1070 K", *25th Symposium (International) on Combustion*, The Combustion Institute, Pittsburgh, in press (1994).

2. Brouwer, J., J.P. Longwell, A.F. Sarofim, R.B. Rarat, and J.W. Bozzelli, *Combustion Science Technology*, Vol. 85, p. 87 (1992).

3. Braker, W., and A. Mossman, *Matheson Gas Databook*, 5th Ed., p. 59, 267 (1971).

4. Corr, R.A., P.C. Malte, and Marinov, *Trans. ASME J. Engineering Gas Turbines and Power*, 114, 425 (1991).

5. Fisher-Porter Manual, Variable Area Flowmeter, Specification Section 1, p. 2 (1991).

6. Glarborg, P., J.A. Miller, and R.J. Kee, *Combustion Flame*, 65, 177 (1986).

7. Koshland, C.P., E.M. Fisher, and D. Lucas, *Combustion Science Technology*, 82, 49 (1992).

8. Kramlich, J. and Malte, P.C., *Combustion Science Technology*, 18, 91 (1978).

9. Miller, J.A. and C.T. Bowman, "Mechanism and modeling of nitrogen chemistry in combustion", *Prog. Energy Combustion Science*, 15, 287 (1989).

10. Reynolds, W.C. and H.C. Perkins, *Engineering Thermodynamics*, fig. B-14a, pg 616 (1977).

11. Safieh, H. Y., J. Vandooren, and P. J. van Tiggelen: *19th Symp. (Int.) Combustion*, p. 117, The Combustion Institute, Pittsburgh (1982).

12. Senecal, Joseph A., *Halon Replacement Chemicals: Perspectives on Alternatives*, Fire Technology, November 1992.

13. *Standards Institute Seeks Potential Halon Alternatives*, Chemical and Engineering News, 1 March 1993.

14. Westbrook, C.K., *19th Symposium (International) on Combustion*, p. 127, The Combustion Institute, Pittsburgh (1982).

15. Westmoreland. P.R., D.R.F. Burgess, W. Tsang, and M.R.Zachariah, "Flouromethan chemistry and its role in flame suppression", *25th Symposium (International) on Combustion*, The Combustion Institute, Pittsburgh, in press (1994).

16. Xieqi, M., B. Cicek, and S.M. Senkan, *Combustion Flame*, 94, 131, (1993).

17. Zentler-Gorden, H.E., Ph.D. Dissertation, University of London (1940).

APPENDIX A

GAS FLOW RATE CALCULATIONS

CH_4 and Air Combustion

The chemical equation for stoichiometric combustion of methane (CH_4) and air is:

$$CH_4 + 2(O_2 + 3.76N_2) \rightarrow CO_2 + 2H_2O + 7.52N_2$$

In order to vary the combustion temperature, excess air was varied during the experimental runs. The gas flow rates using 120% to 130% theoretical air are calculated as follows:

a. **120% Theoretical Air:** The chemical equation for 120% theoretical air is:

$$CH_4 + 2.4(O_2 + 3.76N_2) \rightarrow CO_2 + 2H_2O + (0.4)O_2 + 9.024N_2$$

The molecular mass of the products is:

$$\hat{M} = \frac{1(44.01)+2(18.016)+0.4(32)+9.024(28.02)}{1+2+0.4+9.024}$$

$$\hat{M} = 27.825\ g/gmole$$

The gas constant (R) is determined by dividing the molecular mass into the universal gas constant as follows:

$$R = \frac{8.3143\ J/gmole\ K}{27.825\ g/gmole}$$

$$R = .29881\ J/g\ K$$

Assuming a pressure of 101325 Pa, a temperature of 1750 K, and that the combustion products behave as an ideal gas results in the following density:

$$\rho = \frac{P}{RT} = \frac{101325}{(0.29881)(1750)}$$

$$\rho = 193.77\ g/m^3$$

The total molecular weight of the fuel/air mixture is:

$$1(16.04) + 2.4[32 + 3.76(28.02)] = 345.7 \text{ g}$$

The gas flow rates are then calculated as follows based on a reactor volume of 15.8 cc and a mean residence time of 4 ms:

$$\dot{m}_{prod} = \frac{(193.77 g/m^3)(1.58X10^{-5} m^3)}{0.004 s}$$
$$\dot{m}_{prod} = 0.765 g/s$$

Using the principle that mass is conserved and the fuel and air fractional weights, the methane and air flow rates are as follows:

$$\dot{m}_{CH_4} = \frac{(16.04)(0.765)}{345.7}$$
$$\dot{m}_{CH_4} = 0.0355\ g/s$$
$$\dot{m}_{air} = \frac{(329.66)(0.765)}{345.7}$$
$$\dot{m}_{air} = 0.7295\ g/s$$

b. **Summary:** Using the above equations, the flow rates below were calculated:

Theoretical Air	$\dot{m}_{CH_4}(g/s)$	$\dot{m}_{AIR}(g/s)$
120%	0.0355	0.7295
125%	0.0342	0.7318
130%	0.0330	0.7340

Halon Gases Injected in CH_4/Air Combustion

a. **Bromotrifluoromethane (CF_3Br):** The molecular mass of CF_3Br is as follows:

$$12.01 + 3(19) + 79.90 = 148.91 \text{ g/gmole}$$

The amount of halon injected was based on the following equations:

gmoles retardant/s =

$$\frac{(\#\ \text{gmoles prod})}{(1\ \text{gmole } CH_4)} \times \frac{(\%\ \text{Retardant})}{(\text{gmoles prod})} \times \frac{\dot{m}_{CH_4}}{16.04\ \text{g/gmole } CH_4}$$

$$\dot{m}_{CF_3Br} = \text{gmoles retardant/s} \times 148.91\ \text{g/gmole}$$

Based on the previous fuel/air flow rate calculations, the following applies to the above retardant calculations:

Theoretical Air	# gmoles prod	$\dot{m}_{CH_4}(g/s)$
120%	12.424	0.0355
125%	12.900	0.0342
130%	13.376	0.0330

Therefore, the CF_3Br gas flow rates are as follows:

	Theoretical Air		
% Retardant	120%	125%	130%
0.25	0.0102 g/s	0.0102 g/s	0.0102 g/s
0.50	0.0205	0.0205	0.0205
0.75	0.0307	0.0307	0.0307
1.00	0.0409	0.0409	0.0410
1.50	0.0614	0.0614	0.0615
2.00	0.0819	0.0819	0.0820
2.50	0.1024	0.1024	0.1024
3.00	0.1228	0.1229	0.1229

b. **Trifluoromethane (CF_3H):** The molecular mass of CF_3H is as follows: 12.01 + 3(19) + 1.01 = 70.02 g/gmole

The amount of halon injected was based on the following equations:

gmoles retardant/s =

$$\frac{(\#\ \text{gmoles prod})}{(1\ \text{gmole } CH_4)} \times \frac{(\%\ \text{Retardant})}{(\text{gmoles prod})} \times \frac{\dot{m}_{CH_4}}{16.04\ \text{g/gmole } CH_4}$$

$$\dot{m}_{CF_3H} = \text{gmoles retardant/s} \times 70.02\ \text{g/gmole}$$

Using the same fuel/air flow rate calculations shown previously, the CF_3H gas flow rates are as follows:

	% Theoretical Air		
% Retardant	120%	125%	130%
0.25	0.00481 g/s	0.00481 g/s	0.00482g/s
0.50	0.00963	0.00963	0.00963
0.75	0.01444	0.01444	0.01445
1.00	0.01925	0.01926	0.01927
1.50	0.02888	0.02888	0.02889
2.00	0.03850	0.03852	0.03854
2.50	0.04813	0.04815	0.04817
3.00	0.05776	0.05778	0.05781

APPENDIX B

GAS FLOW ROTAMETER CALIBRATION DATA

The volumetric flow rates of gases through the JSR was monitored using variable area rotameters. A summary of data for those rotameters follows.

Air Rotameter Calibration

The rotameter used had an FP-1/2-27-G-10 variable area glass tube with a 1/2-GUSVT-40 stainless steel float. Per the manufacturer's literature, the maximum flow rate for this glass tube was 1.82 SCFM. Based on the calibration method provided provided in the manufacturer's literature (Fisher-Porter manual), the following calculation was used for calibration:

$$SCFM = SCFM_{STP}\sqrt{\frac{14.7}{P_{OP}}}$$

Where:

P_{op} = Operating Pressure set at 40 psig (54.7 psia)

$SCFM_{STP}$ = Cubic feet per minute at standard temperature and pressure (70 F and 14.7 psia)

To convert from g/s to $SCFM_{STP}$, the following conversion applied using the density of air at STP as 1203.8 g/m^3:

$$SCFM_{STP} = \dot{m}_{AIR}(g/s)\ \frac{60s}{\min}\ \frac{1}{1203.8g/m^3}\ \frac{35.3143CF}{m^3}$$

$$SCFM_{STP} = \dot{m}_{AIR}(g/s)(1.76014)$$

Therefore, the following equation was used for calibration:

$$SCFM = \dot{m}_{AIR}(g/s)\ (1.76014)\sqrt{\frac{14.7}{54.7}}$$
$$SCFM = \dot{m}_{AIR}(g/s)\ (0.912457)$$

Assuming the scale reading is linear at a given inlet pressure, the calculated SCFM was divided into the maximum flow rate of 1.82 SCFM to determine the scale setting. Applying the above to the air flow rates calculated in Appendix A resulted in the following calibration values:

Theoretical Air	$\dot{m}_{AIR}(g/s)$	SCFM	Scale Setting
120%	0.7295	0.6656	36.6
125%	0.7318	0.6677	46.7
130%	0.7340	0.6760	37.1

CH_4 Rotameter Calibration

The rotameter used had an FP-1/8-25-G-5 variable area glass tube (130 scale) with a black glass spherical float. A positive displacement "Wet Test" meter and stop watch was used to measure volumetric flow rates for calibration purposes. Assuming that CH_4 behaves as an ideal gas, the following equation derived from the ideal gas law was used to calculate the mass flow rate using the measured volumetric flow rate:

$$\dot{m}_{CH_4} = \frac{P\,\dot{V}}{R\,T}$$

Where: P = Atmospheric Pressure (101325 Pa)
$\dot{V}$ = Volumetric flow rate measured by meter (m^3/s)
R = Gas Constant (0.51835 J/g K for CH_4)
T = Standard Temperature (294.3 K)

Substituting the known values into the above equation resulted in the following:

$$\dot{m} = \frac{(101325)\,\dot{V}}{(0.51835)(294.3)}$$
$$\dot{m} = 664.207\,\dot{V}(m^3/s)$$

The following calibration data was taken by timing the measurement of 0.3 CF (0.008495 m^3) of gas in the "Wet Test" meter for each scale reading with the inlet pressure maintained at 40 psig:

Scale	Time(s)	$\dot{V}(m^3/s)$	$\dot{m}(g/s)$
30	261.28	3.251e-5	0.0216
35	228.53	3.717e-5	0.0247
40	202.41	4.197e-5	0.0279
45	183.22	4.637e-5	0.0308
50	168.03	5.056e-5	0.0336
55	155.46	5.465e-5	0.0363
60	145.40	5.843e-5	0.0388
65	134.54	6.314e-5	0.0419
70	129.21	6.575e-5	0.0437

Comparing the CH_4 flow rates calculated in Appendix A with the above calibration data resulted in the following fuel rotameter settings:

Theoretical Air	$\dot{m}_{CH_4}(g/s)$	Scale
120%	0.0355	54
125%	0.0342	51
130%	0.0330	49

Halon Calibration Data

The rotameter used had an FP-1/8-25-G-5 variable area glass tube with a sapphire glass spherical float. Similar to CH_4 calibration, a positive displacement "Wet Test" meter and stop watch was used to measure volumetric flow rates for

calibration purposes. Based on a critical pressure of 574.8 psia for CF_3Br and 701.2 psia for CF_3H (Braker and Mossman, 1971) and an operating pressure of 44.7 psia, the compressibility factor of approximately 1.0 was found for both Halon gases (Reynolds and Perkins, 1977). Therefore, both Halon gases were assumed to behave as ideal gases. As a result, the same calibration method used for CH_4 calibration was used to calculate the mass flow rate from the measured volumetric flow rate. The halon gases were calibrated as follows:

a. **CF_3Br:**

$$\dot{m} = \frac{(101325)\,\dot{V}}{(0.05583)(294.3)} \qquad R_{CF_3Br} = 0.05583 J/g\,K$$

$$\dot{m} = 6166.298\,\dot{V}(m^3/s)$$

The calibration readings were as follows:

Scale	Time(s)	$\dot{V}(m^3/s)$	$\dot{m}(g/s)$
8.0	126.78	1.1168e-5	0.0689
9.0	110.81	1.2778e-5	0.0788
10.0	98.03	1.4444e-5	0.0891
11.0	84.34	1.6788e-5	0.104
12.0	76.59	1.8487e-5	0.114
13.0	69.34	2.0420e-5	0.126
14.0	65.67	2.1561e-5	0.133
15.0	58.90	2.4039e-5	0.148

A graph of the above calibration points shown in Figure 15 indicated that the above scale readings could be estimated using a linear relationship. Therefore, for convenience the above scale readings were estimated using the following staight line equation:

$$\text{Scale} = [\dot{m}(g/s)\ \text{X}\ 88.37] + 1.99$$

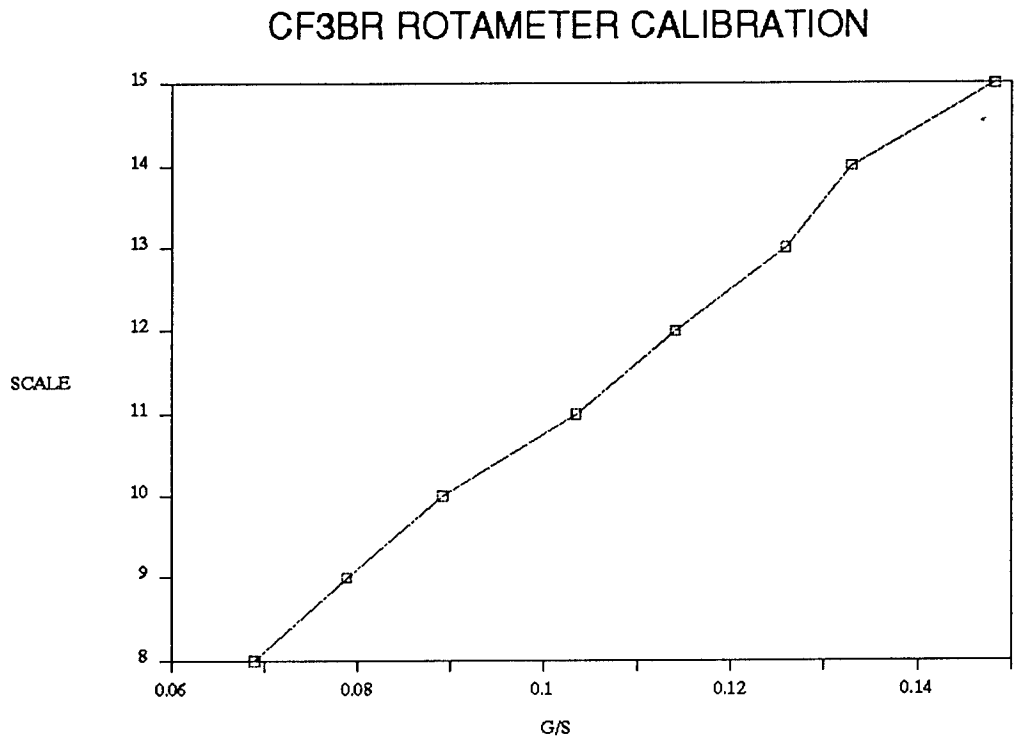

Figure 15: CF_3Br Calibration Graph

b. **CF_3H:** Calibration readings were as follows:

$$\dot{m} = \frac{(101325)\,\dot{V}}{(0.11874)(294.3)} \qquad R_{CF_3H} = 0.11874\ J/g\ K$$

$$\dot{m} = 2899.498\ \dot{V}(m^3/s)$$

Scale	Time(s)	$\dot{V}(m^3/s)$	$\dot{m}(g/s)$
8.0	97.34	1.4546e-5	0.0422
8.5	89.84	1.5760e-5	0.0457
9.0	84.35	1.6786e-5	0.0487
9.5	77.31	1.8315e-5	0.0531
10.0	71.03	1.9934e-5	0.0578
10.5	67.17	2.1079e-5	0.0611
11.0	64.75	2.1867e-5	0.0634
11.5	59.53	2.3785e-5	0.0690
12.0	55.10	2.5697e-5	0.0745

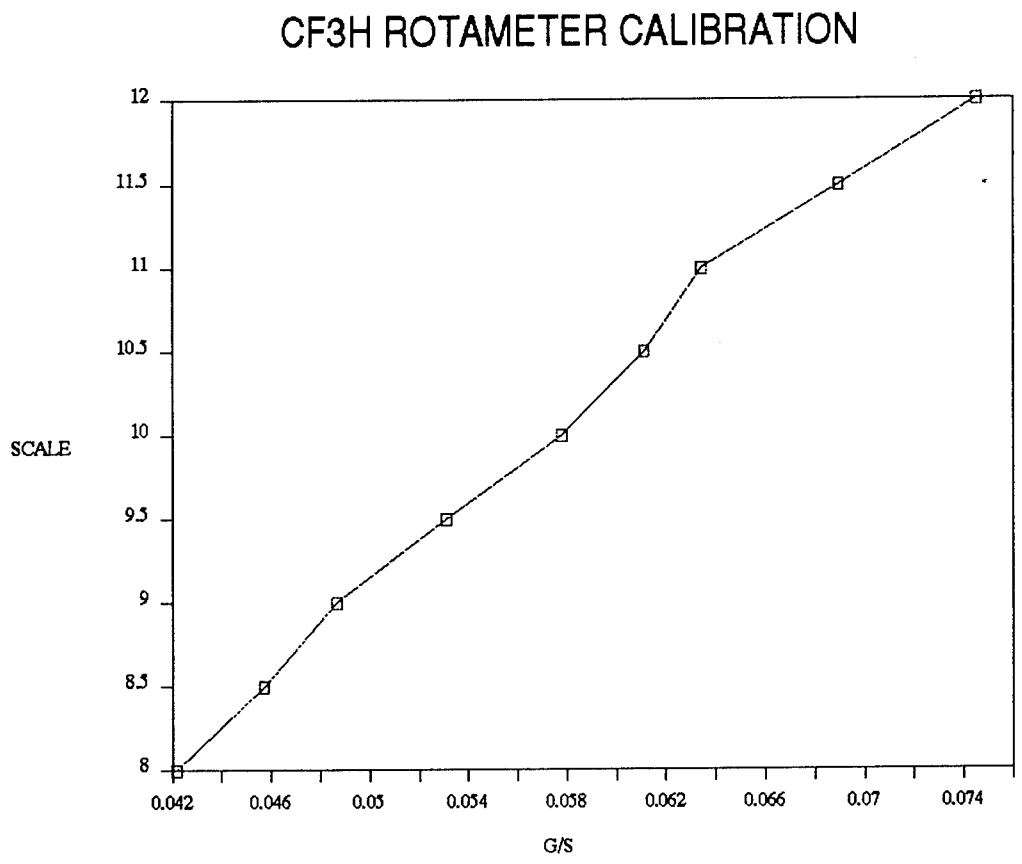

Figure 16: CF_3H Calibration Graph

Similar to CF_3Br, a graph of the calibration points shown in Figure 16 indicated that the these scale readings could be estimated using a linear relationship. Therefore, for convenience the above scale readings were estimated using the following staight line equation:

$$\text{Scale} = [\dot{m}(g/s) \text{ X } 125.90] + 2.79$$

c. **Halon Calibration Summary:** Based on the flow rates calculated in Appendix A, the following rotameter scale settings were calculated:

% Retardant	CF_3Br $\dot{m}(g/s)$	Scale	CF_3H $\dot{m}(g/s)$	Scale
0.25	0.010	2.9	0.0048	3.4
0.50	0.020	3.8	0.0096	4.0
0.75	0.031	4.7	0.014	4.6
1.00	0.041	5.6	0.019	5.2
1.50	0.061	7.4	0.029	6.4
2.00	0.082	9.2	0.039	7.7
2.50	0.102	11.0	0.048	8.8
3.00	0.123	12.9	0.058	10.0

APPENDIX C

GC-FID CALIBRATION METHOD, OPERATING PROCEDURES AND CALIBRATION DATA

Calibration Method

A Perkin Elmer Autosample Gas Chromatograph (GC) with a PE Nelson 1020 Integrator (8088-based computer) were used measure the residual concentrations of halons injected into the jet-stirred reactor (JSR). A Hayes Separation (Haysep) B packed column, six feet in length, was used to measure the halon concentrations. The 1020 Integrator was equipped with software to create data collection and processing methods, and to facilitate report creation and data storage.

A flame ionization detector (FID) mounted in the GC was used to detect and quantify halon concentrations taken from the JSR. Halon concentrations were identified by comparing GC peak areas with those of calibration samples. Since FID response is directly proportional to the number of molecules present in the sample, the sample concentration could be calculated through comparison with FID response to calibration samples.

Calibration samples for concentrations less than 3000 ppm were obtained using a preparation and delivery system consisting of a sample tank, vacuum pump, mercury manometer and associated valves and tubing. The sample tank (Figure 17) consisted of a cylindrical Pyrex glass pipe and stainless steel end plates. Teflon sheets were placed between the plates and the pipe ends to act as gasket material and reduce the possibility of interaction between the steel and compounds in

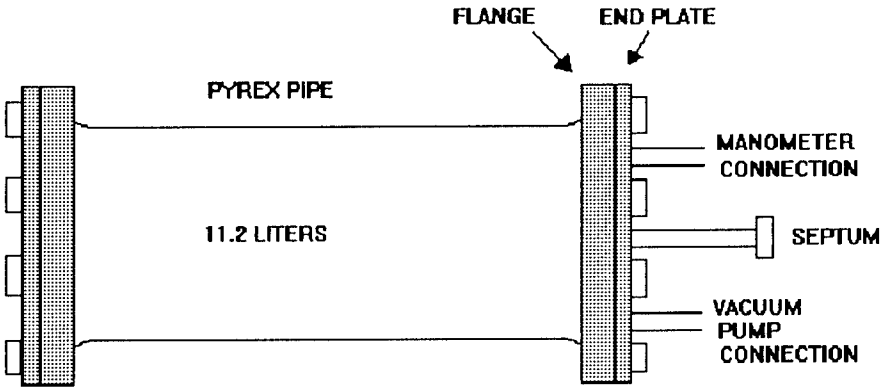

Figure 17: Sample Tank

the tank. Calibration sample makeup began by evacuating the sample tank to less than 0.5 inch Hg. The sample compound was then injected via a gas tight syringe into the tank through the septum and vaporization fitting.

A gas tight syringe with approximately 30 cc capacity was used as a "sample tank" for calibrations greater than 3000 ppm. A gas tight syringe of 1 cc capacity was injected directly into the 30 cc syringe to obtain the desired dilution.

The quantity of gas injected for both methods was based

on the desired ppm for calibration using the following formula derived from the ideal gas law:

$$ppm = \frac{(10^6)(Px)(Vx)}{(Pt)(Vt)}$$

Where: Px = Sample Pressure (atmospheric)
Vx = Sample Volume
Pt = Tank Pressure (approximately 36 inches Hg)
Vt = Tank Volume

For the calibration procedure using injection of gas into the tank, a valve was opened and the tank flooded rapidly to a pressure of approximately 36 inches Hg with room air or nitrogen through an opening centered on one end plate with a diameter about 3% that of the tank. The rapidly filling via a jet into what was initially near vacuum provided the mixing needed to obtain a nearly homogeneous mixture.

For the calibration method in which gas was injected into the 30 cc syringe, the syringe was initially set at 5 cc with room air. After injection of the desired sample size, the syringe volume was increased rapdily to 30 cc with room air to ensure a nearly homogenous mixture.

After the above processes were complete, the mixtures were left standing to allow return to room temperature. Knowing the tank pressure, tank volume, sample pressure and sample volume, the sample compound concentration could be calculated.

The calibration samples were then injected into the GC-FID. After a few seconds to allow the gas in the sample loop to reach GC oven temperature (200 C), the 10 port valve was

rotated allowing pressurized He to force the sample loop contents into the separation column and then through the FID.

The GC used had controls for adjusting the ouput signal level which is referred to as Attenuation. As an example, a setting of 2 meant that the output signal had been attenuated by a factor of two. Due to tendency of the Halon gases to peak out, an Attenuation of 32 was used for calibration.

Calibration Data

Using the procedures described previously, calibration data was collected for CF_3Br and CF_3H as follows with calibration graphs shown in Figures 18 and 19:

a. **Bromotriflouromethane (CF_3Br):**

Vx (cc)	Vt (cc)	Px(in Hg)	Pt(in Hg)	ppm	GC Area
1	30*	30.17	30.17	33,300	6625005
0.8	30*	30.17	30.17	26,700	5653018
0.6	30*	30.17	30.17	20,000	4607950
0.4	30*	30.17	30.17	13,300	3500342
0.2	30*	30.17	30.17	6,700	2028190
30	11,200	30.17	36.87	2,200	682527
20	11,200	30.17	36.27	1,500	474281
10	11,200	30.17	36.27	740	246820
5	11,200	30.17	36.27	370	111362
1	11,200	30.17	36.07	75	22222

b. **Triflouromethane (CF_3H):**

Vx (cc)	Vt (cc)	Px(in Hg)	Pt(in Hg)	ppm	GC Area
1	30*	30.05	30.05	3,300	3768945
0.8	30*	30.05	30.05	26,700	2897621
0.6	30*	30.05	30.05	20,000	2176871
0.4	30*	30.05	30.05	13,300	1495084
0.2	30*	30.05	30.05	6,700	736199
0.1	30*	30.05	30.05	3,300	376926
30	11,200	30.05	36.25	2,200	227152
20	11,200	30.05	36.05	1,500	149522
10	11,200	30.05	36.00	740	77123
5	11,200	30.05	36.00	370	37277
1	11,200	30.05	36.00	75	7656

* - Dilution obtained using gas tight syringe as "tank"

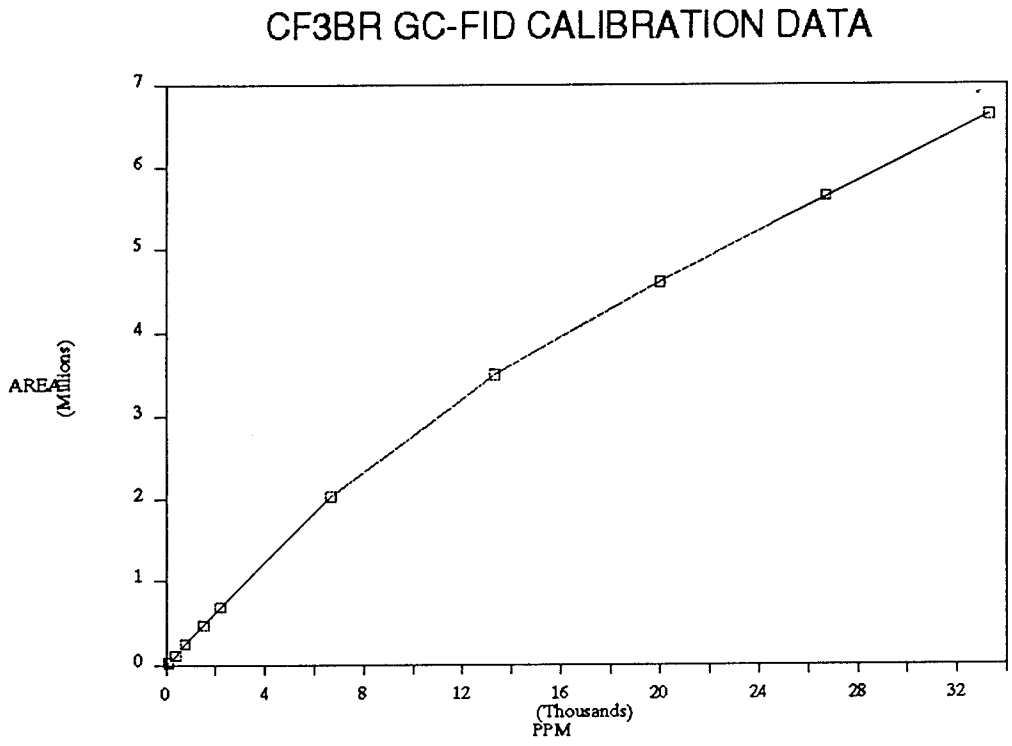

Figure 18: CF_3Br GC-FID Calibration Graph

Operating Procedures

Once the JSR had reached a stable operating point, a 30 cc sample was drawn. The sample was then injected via a stainless steel line into the 10 port valve and sample loop in the GC-FID. Since the GC sample loop has a volume of 1 cc, injection of 30 cc allowed for sufficient flushing out of any air and ensured the sample loop was completely irrigated. The

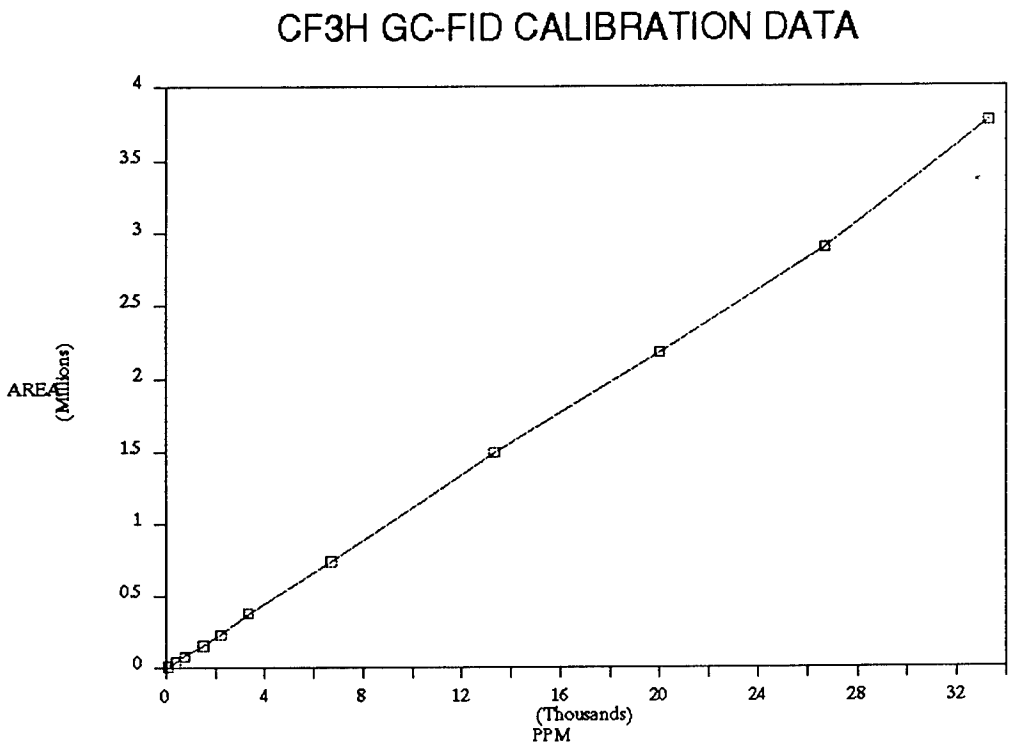

Figure 19: CF_3H GC-FID Calibration Graph

GC was then activated and measurement began. After the sample had completely passed through the GC-FID, the peak area obtained was used to determine concentration.

APPENDIX D

EXPERIMENTAL DATA

Constant Temperature Readings

The following constant temperature readings were taken for preliminary reasons in order to test the experimental system and procedure. It was discovered afterward, that a leak existed in the pre-mixing chamber. Based on locations of the fuel and air lines into the chamber with respect to the leak, it was assumed that leak consisted entirely of air with no fuel or halon gases. Therefore, the following readings represent data that was corrected for the leak based on the O_2 and CO_2 readings taken. The flow rates were also corrected to compensate for the leak.

	% CF_3Br Retardant			
	0	0.5	1.0	1.5
$\dot{m}_{AIR}(g/s)$	0.607	0.595	0.598	0.591
$\dot{m}_{CH_4}(g/s)$	0.0296	0.0273	0.0279	0.0285
% Theoretical Air	120	127	125	121
% CO	0.35	0.32	0.42	0.45
% CO_2	9.2	9.0	9.4	9.9
% O_2	3.8	5.0	4.8	4.2
Temperature (K)	1748	1734	1736	1738

	% CF_3H Retardant		
	0.5	1.0	1.5
$\dot{m}_{AIR}(g/s)$	0.581	0.569	0.553
$\dot{m}_{CH_4}(g/s)$	0.0285	0.0279	0.0273
% Theoretical Air	119	119	119
% CO	0.35	0.37	0.41
% CO_2	9.8	10.1	10.5
% O_2	3.8	4.0	4.0
Temperature (K)	1740	1737	1740

Given that the above data was corrected due to leakage, this data was considered unreliable. Therefore, this data wasn't

used for comparison with the kinetic modeling.

Constant Flow Rate Readings

The following data was taken with the flow rates held constant at 120% theoretical air at flow rates calculated in Appendix A. These readings were corrected to account for the water removed by the impingers by multiplying the data by 0.8481 dry moles/wet mole based on the 120% theoretical air/fuel mixture. The temperature readings were also corrected to account for radiation losses:

% CF_3Br Retardant

	0	0.25	0.5	0.75	1.0	1.5	2.0
% CO	0.15	0.17	0.19	0.23	0.27	0.31	0.59
% O_2	3.6	3.6	3.5	3.6	3.6	3.3	3.3
% CO_2	7.13	7.17	7.04	7.04	7.75	7.56	7.90
NO_x (ppm)	14.0	16.3	15.7	15.7	13.4	15.3	12.3
NO (ppm)	14.4	16.3	15.7	15.3	12.9	15.3	12.3
Temp(K)	1819	1819	1807	1797	1790	1773	1751

% CF_3H Retardant

	0.25	0.50	0.75	1.00	1.50	2.00	2.50	3.00
% CO	0.38	0.40	0.42	0.44	0.42	0.59	0.61	0.65
% O_2	3.6	3.4	3.2	3.0	2.9	2.4	2.4	2.2
% CO_2	7.23	7.31	7.69	8.45	8.89	9.16	9.52	9.87
NO_x (ppm)	16.1	14.8	14.8	15.3	15.3	15.3	15.7	15.7
NO (ppm)	16.1	14.8	15.3	14.8	15.7	15.3	15.7	15.7
Temp (K)	1823	1829	1834	1834	1836	1841	1851	1850

GC-FID readings for all of the above data indicated no residual concentrations of CF_3Br and CF_3H. See Chapter III for discussion on the above data.